An Intriguing Convex Break in the EGRET SED of Mrk 421

Giridhar Nandikotkur[1,2], Keith M. Jahoda[2], M. Georganopoulos[2,3], R. C. Hartman[2], R. Mukherjee[4], D. J. Thompson[2], and Jean H. Swank[2]

ABSTRACT

Based upon analysis of the entire EGRET data from Mrk 421, it is found that the time-averaged spectra are inconsistent with the predictions of current theoretical models that have had success in describing simultaneous X-ray/TeV observations, and suggest additional components in the GeV band, as well as complex time variability. Current theoretical pictures explain the GeV emission as comptonization of the synchrotron photons in the jet, and predict hard spectra that should join smoothly with the TeV emission. Our analysis shows that the situation is more complex. The spectrum ranges from hard to soft during individual epochs, and shows a convex[†] break in the aggregated data. We also present the mission-averaged EGRET spectrum for PKS 2155-304, which shows a similar (but not as pronounced) convex curvature. We discuss a series of possible explanations for the $10^{22} - 10^{23}$ Hz declining part of the EGRET νF_ν spectrum for Mrk 421, and suggest that it is synchrotron emission from the high energy tail of the electron population that produces the X-rays during the highest X-ray states. Such multi-MeV photons are produced by electrons accelerated close to the limit of diffusive shock acceleration. Simultaneous GLAST and X-ray observations of high X-ray states will address the issue of the convex curvature in the future.

---

[1]Department of Physics, University of Maryland at College Park, College Park, MD 20742; giridhar@milkyway.gsfc.nasa.gov

[2]Astrophysics Science Division, NASA Goddard Space Flight Center, Greenbelt, MD, 20771

[3]Joint Center for Astrophysics, University of Maryland at Baltimore County, Baltimore, MD 21250

[4]Department of Physics and Astronomy, Barnard College and Columbia University , New York, NY 10027

[†]We use the mathematical definition of a convex function here. The flux values decrease until the break energy and increase beyond the break.

1. Introduction

The broadband spectral energy distribution (SED) from high-frequency peaked BL Lac objects (HBLs) shows two bumps (Sambruna et al. 1996). The peak at lower frequencies is in the X-ray region, and is widely believed to be due to synchrotron emission from relativistic electrons in the blobs of radiating plasma moving along the jet, away from the core of the active galactic nucleus (AGN). Under the scenario of "leptonic models", wherein the plasma mainly consists of electron and positrons, the second bump is attributed to inverse-Compton scattering of photons that are generated from the synchrotron process itself as postulated by the synchrotron Self-Compton (SSC) models (Maraschi et al. 1992; Marscher & Gear 1985; Bloom & Marsher 1996). These models have had success in fitting simultaneous X-ray and TeV data in many states of activity (Błażejowski et al. 2005). However, model fits for HBLs published in the literature so far have had extremely sparse to almost no coverage in the EGRET energy range, which lies on the rising part of the inverse Compton bump that peaks at TeV energies. HBLs are faint at EGRET energies and individual observations are very often not statistically significant. It is expected that the EGRET HBL spectrum is hard, with a photon index < 2.

However, in our studies, we find that *not all the available EGRET data for HBLs has been accounted for* in the different multiwavelength fits attempted so far in the literature. We have done a comprehensive analysis of the entire data set from the two HBLs: Mrk 421 and PKS 2155-304, which were observed by EGRET multiple times during its nine-year mission. We find that the results contradict the current assumptions about these sources. We describe the analysis in §2, and in Section §3 discuss possible scenarios that explain the intriguing HBL spectrum.

2. Analysis and Results

Following the standard EGRET analysis method (e.g. Hartman et al. (1999) and Nandikotkur et al. (2007)), we extracted the flux at energies >100 MeV, and determined the significance of detection (e.g. as defined in Mattox et al. (1996)) for the HBLs studied in this work. Table 1 gives our results for the different viewing periods (VPs) during which the sources Mrk 421 and PKS 2155-304 were detected. In some cases, temporally close VPs were combined: e.g. V+322.0 (322.0+326.0), V+227.0 (227.0+228.0) to get a stronger significance. Column 5 in Table 1 gives the power-law photon spectral index obtained over the energy range 30 MeV-10 GeV, determined over four to ten energy intervals depending upon the strength of the detection.

Table 1. Details of HBL observations by EGRET.

Source VP[a]	(RA, Dec) MJD Range	Flux[b]	$\sqrt{(TS)}$[c]	Gamma[d]
Mrk 421	(166.10, 38.15)			
0.6	48383.7-386.8	19.7±11.3	2.2	...
4.0	48435.8-449.7	15.6±3.8	5.4	2.07±0.28
40.0	48882.7-903.6	21.6±6.9	4.0	2.01±0.34
V+218.0	49097.6-138.6	11.2±4.5	3.0	
V+227.0	49167.6-195.5	15.1±5.9	3.4	2.68±0.39
326.0	49482.7-489.6	24.4±6.7	5.3	1.47±0.29
V+322.0	49447.6-489.6	13.7±3.3	5.5	1.20±0.27
PKS 2155-304	(329.68, -30.40)			
209.0	49027.8-040.7	15.1±6.9	2.8	
404.0	49671.7-685.6	30.6±7.7	5.9	1.83±0.23
V+513.0	50119.6-231.6	18.3±6	4.0	1.51±0.40
V+701.0	50763.6-777.6	67.7±19.9	4.9	2.35±0.35
V+708.0	50812.6-826.6	30.7±30.7	2.9	1.73±0.49

[a]Viewing periods. V+ indicates a combination of two temporally close viewing periods within the range of dates mentioned. See Hartman et al. (1999) and Nandikotkur et al. (2007) for details.

[b]Flux > 100 MeV, in units of 10^{-8} ph cm^{-2} sec^{-1}

[c]Significance of detection (See Mattox et al. (1996) for definition)

[d]Photon Spectral Index (30 MeV-10 GeV)

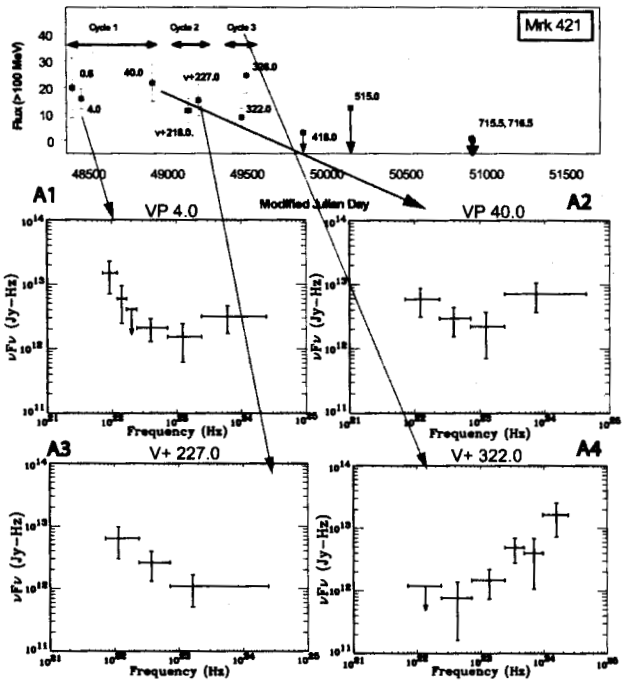

Fig. 1.— EGRET light curve (top figure) and individual spectra for Mrk 421. A wide range of spectral indices can be observed.

Figure 1 shows the light curve for the entire EGRET mission and the νF_ν spectra for Mrk 421. Immediately apparent is the wide difference in the spectral states, also quantified by the range of spectral indices observed (Table 1). The photon index ranges from a hard value of 1.2±0.27 (during V+322.0), to a soft value of 2.68±0.39 (V+227.0). The former shows a rising spectrum (Fig.1-A4), consistent with what is believed about these sources so far. However, the falling trend in the latter spectrum (Fig.1-A3) is unexpected for HBLs.

Even more interesting is the difference between the spectra of VP 4.0 (Fig.1-A1) and V+322.0 (A4). The fluxes recorded during these two sets of observations, both $\sigma 5.4\sigma$ detections (see Table 1), are similar within the error bars, but the νF_ν spectra look very different. In order to get a statistical perspective on how different these spectra are, we performed a series of fits by varying the two free parameters, power-law normalization and spectral index, and plotted the chi-squared values of the fit. The substantial regions of non-overlap in the chi-squared confidence contours (for 1, 2 and 3 σ levels) in Figure 2 illustrate that these spectra are indeed different in spite of the fairly large error bars on the data points.

The fitted values lie just outside the 99% contours of each other. Although the best fit value (2.07 ± 0.28) for VP 4.0 is very close to 2.0, a horizontal line in a νF_ν spectrum, the first five points seem to have a significantly steeper spectrum. The asymmetric shape of the contours around the fitted values also confirmed the preference for softer spectra. We performed a spectral fit for the first five points and obtained a spectral index of 3.18 ± 0.45 and the chi-squared contours for this fit have a very small overlap with those for observations during V+322.0. The curvature introduced in the spectrum by the last data point in Fig.1-A1 suggests the possibility of a convex break, which is a realistic possibility, if a "completely" soft (V+227.0 in A3) and a completely hard (V+322.0 in A4) spectrum coexist in the same energy range. We fit the entire spectrum with a broken power-law by fixing the break energy at the best fit value of 243 MeV, and obtained an F-test probability of 96% for the broken power law being a better fit than the single power law. The indices before and after the convex break were 3.5 and 1.46 respectively.

The spectrum observed during VP40.0 (Fig. 1-A2) is also consistent with this picture. However, the best fit is a horizontal line with spectral index of 2.01 ± 0.34, and the small number of points does not warrant a broken power law fit. The combined spectrum for Mrk 421 in Cycle 1, detected at a signifiance of 7.2σ, makes a stronger case for a convex † break, and is shown in Fig.3. We fit the spectrum with a broken power-law with the break energy fixed at its best value of 235 MeV, and obtained values of 2.89± 0.43 and 1.46±0.18 for the spectral indices below and above the break energy. The F-test probability for the presence of a convex break is 96.7%.

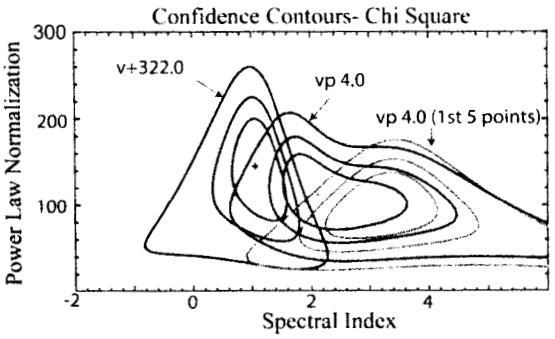

Fig. 2.— 1, 2 and 3 σ Chi-squared confidence contours for power-law fits to spectrum from a hard state (V+322.0) and a soft state (VP 4.0). First 5 points in VP 4.0 are better fit with a steeper index.

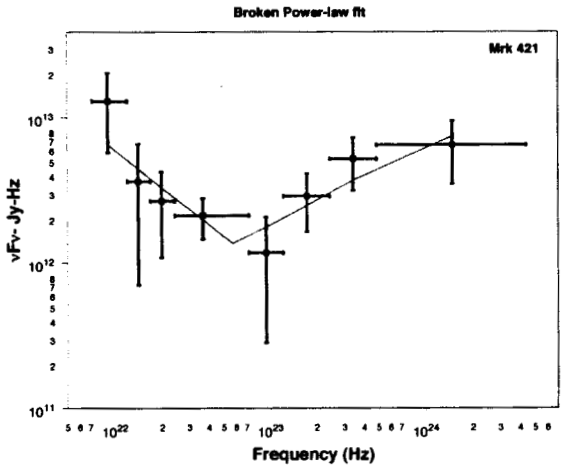

Fig. 3.— A broken power law fit to the convex spectrum during Cycle 1 (a 7.2 σ detection). The indices before and after the break energy (fixed) of 235 MeV are 2.89± 0.43 and 1.46±0.18 respectively.

2.1. The Multiwavelength Picture

Figure 4 shows the broadband SED for Mrk 421 for the EGRET data from from Cycle 1, and the hardest (V+322.0) and the softest (VP 4.0) spectral states. The Whipple data (100 GeV-10 TeV) are taken from Blażejowski et al. (2005) while the STACEE data (130 GeV-1TeV) are from Carson et al. (2006). We obtained the BEPPOSAX X-ray data from the mission website: http://www.asdc.asi.it, and the INTEGRAL spectrum has been taken from the active state of Mrk421 shown in Lichti et al. (2007). We also analyzed all the available data from the PCA instrument on the Rossi X-ray Timing Explorer (RXTE), and extracted spectra (3-20 keV) from the highest and the lowest states recorded during the period 1996-2005. As the X-ray flux increases from the lowest state, the spectral index hardens and the synchrotron peak moves to higher energies. The spectrum from the HEXTE instrument (also on RXTE), extending up to 100 keV, during the highest PCA state is also shown. However, the HEXTE data points are slightly below those of PCA in the overlapping energy interval due to a difference in the relative normalizations. This increases the perceived curvature at higher energies. The spectra from the All Sky Monitor (ASM; 2-10 keV) on RXTE shown in the figure are from the peak state of a day scale light curve labeled as "ASM-day". The "ASM-ind" denote the spectra from individual dwells corresponding to the peak-flux (which has large error bars) and the individual dwell with the highest significance during the same day. The highest ASM state shows an increasing trend, albeit with large error bars on the lowest two points.

The hard EGRET state (V+322.0) shown in the figure is consistent with the EGRET data lying on the increasing phase of the inverse-Compton bump. However, in order to connect the spectrum from the soft state during VP 4.0 to any of the TeV states shown, one would need a convex break at higher EGRET energies. Similarly, the rising part (at higher EGRET energies) of the convex spectrum from Cycle 1 connects smoothly to the TeV data, but the soft spectrum at lower energies is unexpected for HBLs and challenges our current understanding of these sources.

The scenario in case of PKS 2155-304 is a little different. There is no direct evidence of a convex break in the spectrum. The two states VP 404.0 and V+ 701.0, detected at $\sim 5\sigma$ and above, had one hard and one soft (compared to a value of 2.0) spectral index respectively (see Table 1). The latter was from a flare in Nov. 1997, the *SED from which was never published.* We combined all the EGRET data from PKS 2155-304 to see if the anomalous (from the point of view of current models) contribution of the flare disappears. The resultant detection has a significance of 8.0 σ and the spectrum has an index of 2.07 ± 0.15 for a single power-law. However, the spectrum (in Figure 4) is not a power-law, but instead shows a convex curvature (similar to but not as prominent as the Cycle 1 spectrum of Mrk 421). The

TeV data are from the Cerenkov telescope H.E.S.S. (Aharonian et al. 2005).

In order to verify that this convex spectrum is not an artifact of the analysis or characteristic of all gamma-ray blazars, we also looked at the aggregated spectra for 48 other sources that were detected at a significance $> 3.0\,\sigma$. The only source (of the 48) that showed a convex curvature was PKS 2005-489 (detected at 3.0 σ), also an HBL like Mrk421 and PKS 2155-304.

3. Discussion and Conclusions

Mrk 421 definitely shows a convex break in the Cycle 1 time-averaged spectrum and has indications of the same during several different individual epochs. The spectrum has statistically different hard and soft states during its multiple detections. PKS 2155-304 also shows a convex curvature in a nine-year combined EGRET spectrum. This is certainly perplexing from the point of view of leptonic models.

A possible way to explain the convex SED of Mrk 421 is through a third spectral component that would peak at $\nu \sim 10^{21-22}$ Hz ($\epsilon \sim 10 - 100$, where $\epsilon = h\nu/m_e c^2$ is the dimensionless photon energy), and decrease by approximately an order of magnitude by $\nu \sim 10^{23}$ Hz ($\epsilon \sim 10^3$). Such a component could be due to IC scattering of an external photon field. The requirement that the bulk of such a component is confined to $\epsilon \lesssim 10^3$ constrains the seed photon field to energies $\epsilon_{seed} \gtrsim 1/\epsilon \sim 10^{-3}$, due to Klein-Nishina cross-section considerations (Georganopoulos, Kirk, & Mastichiadis 2001). Neither the broad line region ($\epsilon_{seed} \sim 10^{-5}$) nor the putative molecular torus ($\epsilon_{seed} \sim 10^{-6} - 10^{-7}$) photon fields (Blażejowski et al. 2000) satisfy this constraint, so we, therefore, disfavor this possibility.

Another possibility is that the convex feature is still SSC emission resulting from structure in the electron energy distribution (EED). This would require that the EED is convex at $\gamma \sim 10^3$,with a power-law form at higher energies that produces the $\nu \gtrsim 10^{23}$ Hz SSC SED. The resulting SSC convex point would be at $\epsilon \sim (\epsilon_{s,peak}/\delta)\gamma^2\delta \sim 10^3$, where $\epsilon_{s,peak} \sim 10^{-3}$ corresponds to the peak synchrotron energy, while δ and γ are the Doppler factor of the jet and the Lorentz factor of the electrons, respectively. A problem with this interpretation is that no convex point is observed in the synchrotron SED at $\nu \sim 10^{12}$ Hz (for $\gamma = 10^3$, $\delta = 10$, magnetic field $B \sim 0.1$ G). This may be attributed to the possibility that the synchrotron SED at that frequency is dominated by emission at larger ($\sim$ pc instead of $\sim 10^{-2}$ pc) spatial scales. Another problem this mechanism faces is that when the low energy EED varies, one expects that the EED at $\gamma \gtrsim 10^3$ varies as well. Variations, therefore, of the steep low energy EGRET emission should be accompanied by variations of the hard high

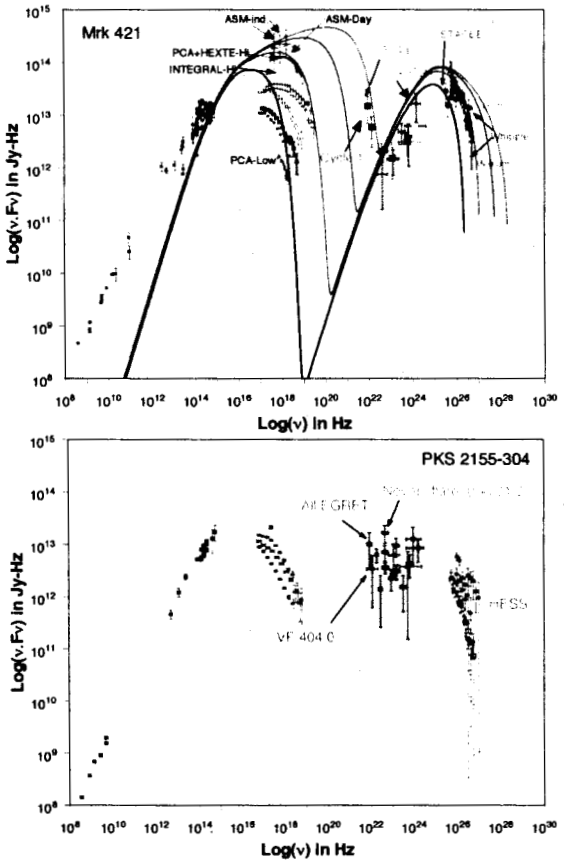

Fig. 4.— Multiwavelength SED for Mrk 421 and PKS 2155-304. Solid curves for Mrk 421, depict model SEDs of increasing values of $\eta = 3.4 \times 10^5$, 1.4×10^4, 3.4×10^3, 5.4×10^2, 34, for a homogeneous source of radius $R = 10^{16}$ cm and $\delta = 10$, permeated by a magnetic field $B = 0.5$ G.

energy EGRET emission. This, however, is not observed, as can be seen in Figure 1, where during Cycle 3 the soft low energy EGRET SED has disappeared, while the hard high energy EGRET component is very pronounced.

We examine now the possibility that the low energy EGRET emission is the high energy tail of the synchrotron component. During high X-ray states of TeV blazars, the X-ray spectrum becomes harder, and several instances have been observed of sources that exhibit flat or even rising SEDs up to $\sim$ 100 keV, the maximum energy reachable by X-ray telescopes (e.g. Mrk 501, 1ES 1426+428, 1ES 2344+514; (Costamante & Ghisellini 2002)). This behavior, expected from episodic particle acceleration (Perlman et al. 2005), also characterizes Mrk 421, as can be seen in Figure 4. The upper limit (e.g. Guilbert et al. (1983)) of the frequency of synchrotron radiation produced via diffusive shock acceleration can be obtained by equating the acceleration rate $t_{acc}^{-1} = c/\eta R_L$, where $R_L = m_e c\gamma/eB$ is the Larmor radius of an electron with Lorentz factor γ in a magnetic field B and $\eta \geq 1$, to the radiative loss rate $t_{rad}^{-1} = \sigma_\tau \gamma B^2 (1 + (L_c/L_s))/(6\pi m_e c)$, where L_s and L_c are the synchrotron and inverse Compton luminosities of the source. This results to: $h\nu_s = 9\delta m_e c^2/4\eta\alpha(1 + L_c/L_s) \approx 150\delta/(\eta(1 + L_c/L_s))$ MeV, where $\alpha \approx 1/137$ is the fine structure constant, and the upper limit is obtained for $\eta = 1$. Extreme synchrotron acceleration has been observed in the case of the Crab nebula (e.g. de Jager et al. (1996)), in which the synchrotron SED peaks at the optical, beyond which it extends as a power-law up to $\sim$ 30 MeV, suggesting $\eta \sim 1$ for this synchrotron dominated source. The possibility of extreme acceleration in blazars has been discussed by Ghisellini (1998), who suggested that the so-called blazar sequence (Fossati et al. 1998) may extend to powers significantly lower than those of the TeV blazars, producing strongly synchrotron dominated sources with synchrotron SEDs peaking up to $\sim$ 200 MeV.

It is possible, however, that Mrk 421 is the first identified extreme extragalactic accelerator and one does not have to stretch the blazar sequence to look for such sources. An extragalactic extreme accelerator does not need to produce a synchrotron SED that peaks at MeV energies. An equally valid, and physically more plausible picture is the one exhibited by Crab, namely that, although the peak of the synchrotron component is at lower energies, the synchrotron SED extends to MeV energies, and is produced by electrons that after being accelerated, cool radiatively before they escape from the source (Kirk, Rieger, & Mastichiadis 1998). In the case of Mrk 421, as can be seen from Figure 4, as the X-ray flux increases the X-ray spectrum becomes harder, and it is possible that at the highest X-ray states the synchrotron spectrum extends and joins smoothly with the lower energy portion of the EGRET spectrum. This is demonstrated with the solid curves in Figure 4 that depict model SEDs for increasing values of η. In this scenario, the steep synchrotron emission can dominate over the hard SSC spectrum in the lower EGRET energies during the brightest

X-ray states. This steep $\nu \lesssim 10^{23}$ Hz emission will be more variable and will not correlate well with the $\nu \gtrsim 10^{23}$ Hz SSC variations that are expected to be slower and of smaller amplitude. A hint of this behavior can already be seen in Figure 1. Note that from all the X-ray states depicted in Figure 4, only the highest ones seem to have the potential of connecting smoothly to the steep EGRET SED. This raises the issue of duty cycle that can be addressed through simultaneous GLAST and X-ray observations of Mrk 421 and other TeV blazars. Such observations will help us evaluate our suggestion that TeV blazars are extragalactic transient extreme accelerators.

REFERENCES

Aharonian, F., et al. 2005, A&A, 430, 865

Błażejowski, M., et al. 2000, ApJ, 545, 107

Błażejowski, M., et al. 2005, ApJ, 630, 130

Bloom S. D., & Marscher, A. 1996, ApJ, 461, 657

Carson, J. et al. 2007, ApJ, 662, 199

Costamante, L. & Ghisellini, G. 2002, A&A, 384, 56

Fossati, G. et al. 1998, MNRAS, 299, 433

Georganopoulos, M. Kirk, J. G. & Mastichiadis, A. 2001, ApJ561, 111

Georganopoulos, M. & Kazanas, D. 2003, ApJ, 594, L27

Ghisellini, G. 1998, Astroparticle Physics, 11, 11

Ghisellini, G., Tavecchio, F. & Chiaberge, M. 2005, A&A, 432, 401

Guilbert, P. W., Fabian, A. C., & Rees, M. J. 1983, MNRAS, 205, 593

Hartman, R. C., et al. 1999, ApJS, 123, 79

Kirk, J. G., Rieger, F. M., & Mastichiadis, A. 1998, A&A, 333, 452

de Jager, O. C. et al. 1996, ApJ, 457, 253

Lichti, G. et al. http://arxiv.org/pdf/0704.2338

Mattox, J.R. 1996, ApJ, 461, 396

Maraschi, L., Ghisellini, G., & Celotti, A. 1992, ApJ, 397, L5

Marscher, A.P., & Gear, W.K. 1985, ApJ, 298, 114

Nandikotkur, G., et al., 2007, ApJ, 657, 706

Perlman, E. S. et al. 2005, ApJ, 625, 727

Sambruna, R. M., Maraschi, L., & Urry, C. M. 1996, ApJ, 463, 444